Supporting Information

Polymer conformational entropy as driver of complex coacervation

Tommaso Inzani[a], Giovanni Nava[a], Marco Buscaglia[a], Andrea Soranno[b], Alessandro Gori[c], Greta Bergamaschi[c], Samir Suweis[d, e], Amos Maritan[d, e, 2], Tommaso Bellini[a, 1]

[a]Dipartimento di Biotecnologie Mediche e Medicina Traslazionale, Università degli Studi di Milano, 20133 Milano, Italy
[b]Department of Biochemistry and Molecular Biophysics, Washington University in Saint Louis, 63110 Saint Louis, Missouri, USA
[c]Istituto di Chimica del Riconoscimento Molecolare, Consiglio Nazionale delle Ricerche, 20131 Milano, Italy
[d]Dipartimento di Fisica e Astronomia, Università degli Studi di Padova, 35121 Padova, Italy
[e]Istituto Nazionale di Fisica Nucleare, Sezione di Padova, 35121 Padova, Italy

Corresponding authors: [1] tommaso.bellini@unimi.it
[2] amos.maritan@unipd.it

S1 Sample composition and preparation

S1.1 RNA polymers

As polyanion we chose the least structured, most ideal RNA chain, *i.e.* the homopolymeric single stranded Polyuridylic acid potassium salt (PolyU), which we purchased from Merck, Germany (P9528). These PolyU chains, as producer specifications, are polydispersed, with a molecular weight distribution in the range 100-1000 kDa as measured by electrophoresis and LALLS, and variations among lots. PolyU solutions were prepared in 150 mM NaCl using RNAse free Milli-Q pure water, and buffered at pH 7 with 20 mM Tris-HCl buffer. PolyU solutions were stored at -20 °C to avoid degradation. PolyU, as a RNA chain, is negatively charged at the expoled pH. We considered the total chain charge Q_{PolyU} to be equal to the monomer number of the chain.

S1.2 Cationic peptides

Experiments were performed investigating the effect of three different positively charged peptides. Two are homopolymers, Poly-L-Lysine hydrobromide, of different average molecular weight $\langle MW \rangle$ (ranging between 1-5 and 4-15 kDa as producer specifications) and with an average degree of polimerization of 15 and 45 residues, indicated as PLL15 and PLL45 (Merck, Germany P0879 and P6516 respectively).

A third peptide, meCP, was synthesized based on literature studies that demonstrated its phase behavior when mixed with PolyU RNAs [1]. The peptide sequence, $[SR]_4E\underline{N}LYFQ\underline{G}[SR]_4$ (MW = 2.8 kDa), bearing methyl groups on the backbone nitrogen of glycine and asparagine residues, follows the sticker-and-spacer architecture. The heterotypic interaction with PolyU are indeed mediated by the positively charged arginine residues found in the tail moieties of the molecule. Solutions were prepared at fixed concentrations in 150 mM NaCl and stored at 4 °C to prevent aggregation.

S1.3 Peptide synthesis

maCP peptides were synthesized by fully automated microwave-assisted Fmoc-SPPS on a Biotage ALSTRA Initiator+ peptide synthesizer, operating in a 0.2 mmol scale. Coupling steps were performed for 10 minutes at 60 °C, using Oxyma/DIC as activators. Fmoc- deprotection steps were performed by treatment with a 20% piperidine solution in DMF at room temperature (1 x 10 min). Upon complete chain assembly, the resin-bound peptide was cleaved with an ice-cold TFA-based mixture, and the crude peptide collected by precipitation in cold ether. Analytical RP-HPLC was performed on a Shimadzu Prominence HPLC (Shimadzu) using a Shimadzu Shimpack GWS C18 column (5 micron, 4.6 mm i.d. x 150 mm). Preparative RP-HPLC was performed on a preparative Shimadzu HPLC using a Shimadzu Shimpack G15 column (10 micron, 20 mm i.d. x 250 mm). Pure RP-HPLC fractions (> 95%) were analyzed by ESI-MS, combined, and lyophilized.

S1.4 Sample preparation

In vitro liquid-liquid phase separation (LLPS) was obtained by mixing RNA solutions at fixed concentration with various amounts of peptides, corresponding to various total charge ratios q^+/q^-, where q^- and q^+ are respectively given by $c_{RNA}Q_{RNA}$ and c_pQ_p. In all experiments peptide was added to previously solubilized RNA.

Light scattering measurements on dispersed, un-aggregated PolyU chains (a condition obtained both when the sample is homogeneous and in the dilute phase of a phase separated system), were performed using a set of identical PolyU solution samples prepared in a set of scattering tubes. Experiments were performed with PolyU concentration of $c_{RNA} = 13.5$ μM (≈ 1.5 g/L), a choice of compromise in which solutions are dilute enough to be safely below overlap concentration c^*_{RNA} (see section S3.3) and concentrated enough to provide reliable light scattering signal even during phase separation, when the concentration of solubilized chains is reduced.

We performed light scattering measurements on the RNA solutions from sets of identical samples prepared from the same batch before adding peptides to ensure that all samples in all tubes were indeed equal in scattered intensity and measured diffusion coefficient. We adopted a strict threshold, discarding all samples that differed more than 5% from the mean value of the set, in this way providing a quality

control on the actual concentration in the PolyU solutions and on the uniformity of the glass walls in the scattering tubes. Following this quality check, the same volume of differently concentrated peptide solutions were added in each tube to reach a final peptide concentration c_p. c_p in scattering samples having a charge ratio $0 < q^+/q^- < 1$ was in the range 26.5-636 μM for meCP, 13-309 μM for PLL15 and 4-97.5 μM for PLL45. We also routinely verified that the LS measuring conditions (optical alignment, detection settings) remained stable in all the measurements. This was done by ensuring that the behaviour of standard PolyU solutions remained unaltered across the experimental campaign.

After addition of the peptides, the samples were allowed to equilibrate at room temperature. Equilibration, sped up by gentle sonication cycles, took from a few hours to up to few days for the samples with the largest c_p. The main reason for such slow equilibration is the recovery time from transient non-equilibrium LLPS occurring when denser peptide droplets are added to the PolyU solutions. After sufficient waiting, sedimentation of the dense phase was sped up by two 20 minutes cycles of gentle centrifuging.

Light scattering measurements on condensate samples were performed on the dense phase of samples composed of $c_{RNA} = 135$ μM PolyU with PLL45 at a concentration chosen to balance the PolyU negative charge. Separation was sped up by gentle centrifuging.

S2 Experimental techniques

S2.1 Static and dynamic light scattering

Static light scattering (SLS) and dynamic light scattering (DLS) measurments were performed using a custom-built setup. A solid state Nd:Yag collimated laser beam of wavelength $\lambda = 532$ nm is focused in the center of a scattering chamber after passing through a spatial filter that uses a 20X objective and a vertical polarizer. Light scattered at 90° is detected using a 3 μm core multimodal, optical fiber focused at the center of the chamber. The signal is then optically split (50:50) before being detected by discriminated photomultiplier tubes (Hamamatsu) and processed by a digital correlator (flex-03d, correlator.com) that crosscorrelates the two channel signals. Data are acquired through a custom LabVIEW (National Instruments) software.

Measurements of scattered intensity and of time autocorrelation functions in dilute solutions of PolyU chains (with and without peptide decorations) were performed with 40-45 μL samples directly prepared in cylindrical borosilicate glass capillary (O.D. = 3 mm I.D. = 2.4 mm) flame sealed at one end, purchased from Hilgenberg GmbH (referred in the text as "scattering tubes"). Scattering tubes were immersed in a refractive index-matching water bath contained in a quartz cuvette during data acquisition.

The average scattered intensity $\langle I \rangle$ was obtained by averaging the array of scattered intensities measured at fixed intervals by the correlator. Values of $\langle I \rangle$ presented

in this work are averages of intensity traces having duration of about 2000s. Since the size of the individually solubilized PolyU coils considered in this work are much smaller than λ, the average scattered intensity is a probe of the concentration c_{RNA} of solubilized PolyU, *i.e.* $\langle I \rangle \propto c_{RNA}$. Thus the measurement of $\langle I \rangle$ in samples after equilibration and sedimentation of the dense phase enables determining the concentration of PolyU in the dilute phase: $c_{RNA,s}/c_{RNA} = \langle I \rangle / \langle I \rangle_0$, where c_{RNA} and $\langle I \rangle_0$ are the PolyU concentration and the scattered intensity in the absence of peptide, respectively. In this regime of small scatterers, changes in PolyU coil radius do not affect the scattered intensity. At peptide concentrations large enough to induce phase separation, we perform LS measurements either in the dilute phase in the case of samples prepared at $c_{RNA} = 13.5$ μM in the scattering tubes, or in the dense phase in the case of samples prepared at $c_{RNA} = 135$ μM in thinner capillaries. In the former case, the measurement of c_{RNA} via $\langle I \rangle$ enables determining the PolyU concentration of the dilute phase, and from that the amount of PolyU that has collapsed in the dense phase. The proportionality between $\langle I \rangle$ and c_{RNA} does not hold in the dense phase since in that condition the PolyU coils cannot be considered independent scatterers.

With the same setup we also performed dynamic light scattering experiments in the dense coacervate phase. Correlations were acquired at fixed angle (90°). Given the small volumes available of that phase, samples were confined in thinner capillaries (O.D. = 1.5 mm, I.D. = 900 μm, Merck, Germany Z611255) to gain in the vertical extension of the sedimented dense phase. Approximately 50 μL of charge balanced RNA/peptide sample solution were obtained by mixing RNAs and peptides stock samples directly into the capillary, yielding a ≈3 mm high dense phase volume in the capillary. Light oil was deposited above the sample in the capillary to prevent evaporation and the capillary was flame-closed. The capillary was immersed, during data acquisition, in a refractive index-matching water bath that helped also in thermal stability. Temperature was cycled in the 30-50 °C range. For each temperature step, after a 2 hours thermalization time, five to ten correlations were acquired, each lasting from from 100 o 700 seconds depending on samples ergodicity.

S2.2 Confocal microscopy

As a preparatory step for confocal microscopy, we explored samples by brightfield microscopy. To this aim we confined 1-2 μL droplets between two microscope slides held 10 μm apart by glass spacers.

Confocal microscopy was performed using a Leica DMI600B scanning confocal microscope equipped with 5X and 40X, 60X oil immersion objectives. Observations were performed on 13.5 μM PolyU and peptide samples deposited on the bottom of an imaging 96-well plate (Corning) and covered in light mineral oil to prevent evaporation. The peptide component of the solution contained a 1% fraction of fluorophore-tagged peptides.

Samples were imaged after equilibration and complete sedimentation of the dense coacervate phase on the bottom of the well, that typically required 1-2 days. Samples

were illuminated at $\lambda_{abs} = 490$ nm, to maximize absorption by FAM labeled meCP. Confocal images were analyzed by a MATLAB script to compute the total volume of the dense phase combining and averaging various (4 or 5) fields of view. Volume fractions were retrieved based on the known total sample volume.

S3 PolyU characterization via dynamic light scattering

S3.1 PolyU length determination via static light scattering

Since the characterization of the PolyU used in this work as performed by the producers indicates a highly polydispersity in length, and since the interpretation of the observed phenomena requires knowing the average polymer length N, we resolved to measure $\langle N \rangle$ by light scattering, a choice that grants an homogeneity of procedures and sample treatment. Indeed, the measurement of the light scattering cross section is an accurate tool to determine the molecular mass of the scatterers [2]. To this aim it is necessary to either use a set-up with an absolute calibration, or - more simply - to perform comparative measurements with a suitable reference system, which in our case was a solution of DNA poly-thymine of length 100 (T100). This system was chosen for a combination of reasons: it was produced by solid-state synthesis (from Merck, Germany), so that the polydispersity is minimal and the length is accurately known; it is a DNA rather than a RNA chain, which minimizes issues related to the stability of the system toward potential enzyme degradation; thymine and uracil have a very similar chemical structure, ensuring equal optical polarizability, as also indicated by their very similar UV absorption spectra [3]; thymidine and uridine monomers have an almost identical molecular mass (the difference being less than 1%).

Both PolyU and T100 have a coil size much smaller than the wavelength of the probing light, ensuring that the scattering process is within the so-called Rayleigh regime. This regime is obtained when the oscillating dipoles induced by the illuminating beam within each coil are so close to one another that the scattered waves can be considered as having equal phase. In the Rayleigh regime, the scattered intensity from a dilute polymer solution does not depend on the scattering angle and its value is

$$\langle I \rangle = C_{sc}\, \nu\, \alpha_m\, m^2 \tag{S1}$$

where ν is the number density of polymer scatterers, α_m is the polarizability of each monomer in the chain, m is their molecular mass, and C_{sc} is a constant relative to the setup (illumination, detector sensitivity, light collecting etc). Here we exploit the fact that we are comparing two samples in which α_m is the same that are measured in equal experimental conditions, granting that C_{sc} is also equal. Therefore

$$\frac{\langle I\rangle_{PolyU}}{\langle I\rangle_{T100}} = \frac{\nu_{PolyU}\, m^2_{PolyU}}{\nu_{T100}\, m^2_{T100}} \tag{S2}$$

Since the product $\nu\, m$ is the mass concentration, and since the molecular weight of thymidine and uridine are comparable, the equality above transforms into

$$\frac{\langle I\rangle_{PolyU}}{\langle I\rangle_{T100}} = \frac{c_{PolyU}\, \langle N\rangle_{PolyU}}{c_{T100}\, \langle N\rangle_{T100}} \tag{S3}$$

To remove further experimental uncertainties, we prepared solutions of T100 that give roughly the same value of $\langle I\rangle$ as for the PolyU solutions used in this work. Specifically, with a $c_{T100} = 9$ mg/ml, a condition of independent dilute chains (see section S3.3), we measure $\langle I\rangle_{T100} = 47.2$ kHz, while with $c_{PolyU} = 3$ mg/ml we measure $\langle I\rangle_{PolyU} = 56.3$ kHz. Thus we obtain

$$\frac{\langle N\rangle_{PolyU}}{\langle N\rangle_{T100}} \approx 3.6 \tag{S4}$$

indicating that the length of PolyU is $\langle N\rangle \approx 360$.

We would like to emphasize that this measurement is based on polarizability and mass, and does not depend on geometrical features, such as persistence length, gyration radius or ideal *vs.* non-ideal coil geometry, nor it depends on ionic strength.

S3.2 Measurement of hydrodynamic radius

The hydrodynamic radius of PolyU was measured by dynamic light scattering. The diffusion coefficient D of PolyU coils was determined from the time dependence of the correlation function of the scattered electric field $g_1(\tau) = \langle E(t)E(t+\tau)\rangle$. In the case of monodisperse scatterers $g_1(\tau) = e^{-\Gamma\tau}$, where $\Gamma = Dq^2$, q is the scattering vector ($q \approx 22\ \mu\text{m}^{-1}$) and $D = k_BT/6\pi\eta R_h$, as per the Stokes equation (with η water viscosity and k_B Boltzmann constant) through which R_h is defined.

DLS experiments measure the autocorrelation function of the scattered intensity $g_2(\tau) = \langle I(t)I(t+\tau)\rangle$ [4]. In homodyne conditions $g_1(\tau)$ and $g_2(\tau)$ are related by the Siegert relation $g_2(\tau) = 1 + \beta_0|g_1(\tau)|^2$. The coherence factor β_0 depends on the number of supported modes of the collecting optical fiber. In the setup used in these experiments $\beta_0 \approx 0.45$. Thus, in simple homodyne conditions, R_h is determined by fitting the measured intensity correlation function as:

$$g_2(\tau) = 1 + \beta_0 e^{-2\Gamma\tau}. \tag{S5}$$

Despite the care we put in collecting only the light coming from the interior of the scattering tubes, we could not avoid collecting some stray light, probably due to scattering from the tube walls. Although such stray light is quite dim, it becomes relevant in our experiments because of the low scattering signal from the dilute solution.

The presence of stray component (I_s) added to the fluctuating scattered component (I_f) in the collected scattered light $I_t = I_f + I_s$, results in a decrease of

$\langle I^2\rangle/\langle I\rangle^2$ and hence of an apparent coherence factor β smaller than the value β_0 expected for a homodyne detection. In the experiments we find $1.45 \leq b \leq 1.25$, the lowest values found at largest peptide concentration, when the scattering from the dilute phase is smallest.

The intensity correlation function, in such heterodyne condition, becomes [5]:

$$\begin{aligned} g_{2,H}(\tau) &= 1 + \frac{\beta}{(I_f + I_s)^2}\left[I_f^2 \left|g_1(\tau)\right|^2 + 2I_f I_s \left|g_1(\tau)\right|\right] \\ &= 1 + \beta\left[\frac{1}{(1+x)^2}\left|g_1(\tau)\right|^2 + \frac{2x}{(1+x)^2}\left|g_1(\tau)\right|\right] \end{aligned} \tag{S6}$$

where $x = I_s/I_f$. This method allows to correctly estimate only the light diffused from the sample therefore, since $\langle I_f\rangle \propto c_{RNA}$, the molecular concentration of the sample. We thus fitted the measured intensity autocorrelation function according to Eq. S6 by adopting a simple exponential decay and using τ and x as fitting parameters. For simplicity, both in this document and in the main text the average fluctuating scattered intensity will be referred as $\langle I\rangle$. In Fig. S2a we show an example of $g_2(\tau)$ fitting (green dashed line), where we also plot the difference between data and fitting line (green dots, right-hand side y axis). On average, fitting the data from PolyU samples before the addition of peptides according to Eq. S6 leads to correlation times smaller than those obtained with the simple fitting in Eq. S5 by about 32%.

S3.3 PolyU as a random coil

Dilute PolyU chains in solution assume an open coil conformation, which can be described by a non-self avoiding polymer model [6]. The homopolymeric single stranded sequence of PolyU prevents the formation of secondary structures that would stiffen the chains. Moreover, uracil provides the smallest molecular area among ribonucleic bases, yielding the smallest stacking force, which reflects in a larger flexibility than other homopolymeric RNA as PolyA and PolyC [7]. Thanks to the absence of secondary structures, the conformational properties of independent PolyU coils are dictated by the electrostatic repulsion between its monomers charged moieties and by some residual attraction from stacking of uracils.

Experiments here reported were performed at 150 mM NaCl and 20 mM Tris-HCl, corresponding to a Debye screening length $\lambda_D \approx 7$ Å. The high charge screening allows the coil for an high bending freedom, overcoming the nucleic acid rigidity provided by the fully charged phosphate backbone at physiological pH. Thus, we can describe the RNA polymer using a simple model of random coil:

$$R_g = \frac{\sqrt{N_b}b}{\sqrt{6}} = \sqrt{\frac{2L\xi_p}{6}} \tag{S7}$$

composed of N_b Kuhn segments of length b, with a total contour length L and in which ξ_p is the persistence length. We argue that this assumption, unavoidably an

approximation, is however adequate to the aim of this work, which does not depend on the detailed description of the coil structure of PolyU.

From the length estimate $N \approx 360$ using the comparative measurements described in section S3.1 and equation S7, we obtain an estimate of the persistence length $\xi_p = b/2 \approx 11$ Å, in agreement with different studies of the elasticity of PolyU ssRNA PolyU chain at high enough salt [6, 8, 9]. Moreover, we can safely assume the initial PolyU samples, at the concentration used through the experiment, as a dilute RNA solution being well below the overlap concentration $c^* = m_{PolyU}/1.33\pi R_g^3 \approx 70$ g/L $\gg 1.5$ g/L.

The ratio $\zeta = R_h/R_g$ between hydrodynamic and gyration radii is known to depend on the geometry of the diffusing scatterers. For linear unstructured flexible polymers in theta solvent, theory [10, 11, 12] and experiments [13] indicate such ratio to be $\zeta \approx 0.66$, a value that we adopted in the analysis of our data.

Measurements have been performed at room temperature (T = 25-30 °C). R_h of both bare and peptide-decorated PolyU is nearly independent on T (Fig. S1 and Fig. S4), which hence doesn't need to be accurately controlled.

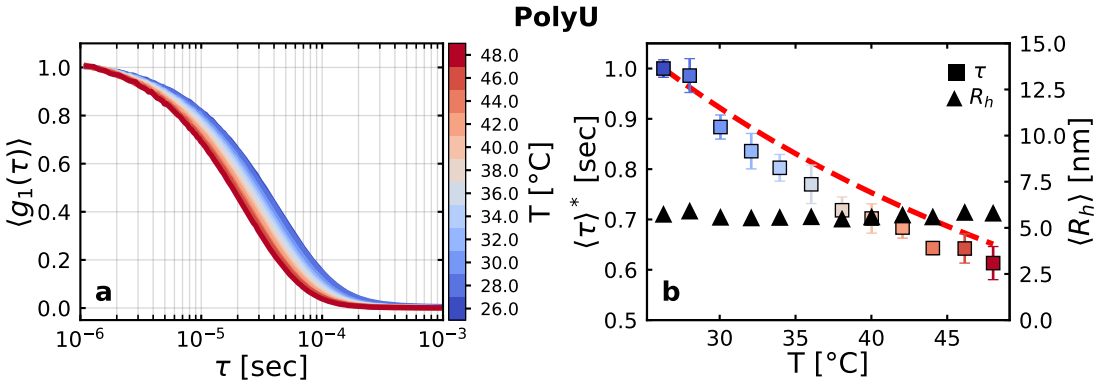

Figure S1: Temperature scan of PolyU DLS measurements. Panel (a) reports the average $g_1(\tau)$ correlation functions acquired in a 25-50 °C temperature range. Panel (b) presents the corresponding normalized fitted relaxation times ($\langle\tau\rangle^*$ colored squares, left axis) and extracted hydrodynamic radius ($\langle R_h\rangle$ black triangles, right axis). The red dashed line corresponds to the normalized water viscosity η dependence on temperature. Relaxation times trend does not deviate significantly from water viscosity, indicating the independence of PolyU coil radius from the temperature in the explored range.

S3.4 Polydispersity of PolyU

Although the fitting of $g_2(\tau)$ with a single exponential decay in the heterodyne regime is a good approximation, as visible in the figure, and it will be used throughout the analysis of this work, we carried out an investigation on the length polydipersity of PolyU by analyzing the deviation between the data and the best fitting curve according to Eq. S6, which can be appreciated in Fig. S2b, where a zoom of panel S2a is shown (yellow shading).

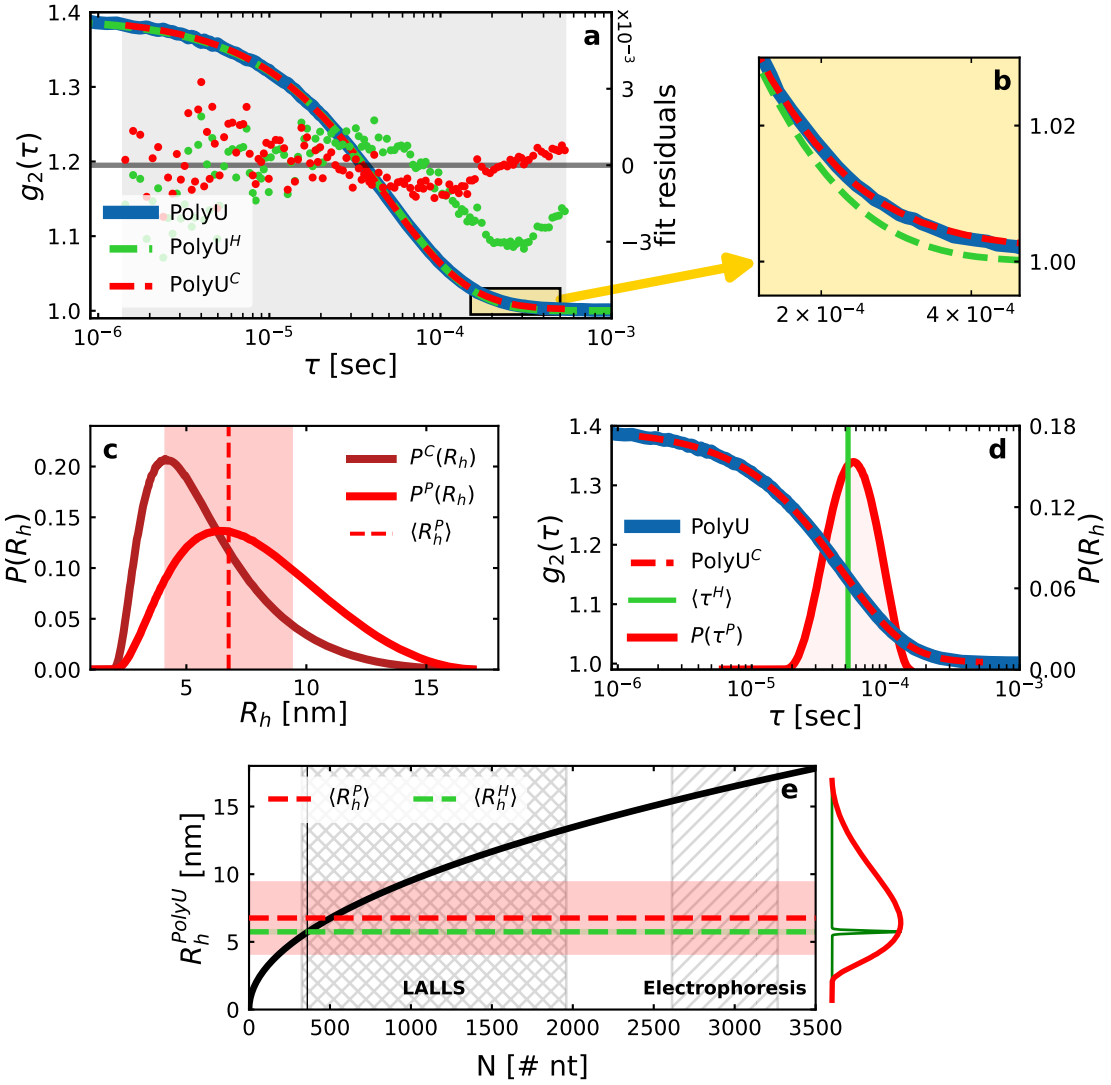

Figure S2: Data analysis of PolyU DLS measurements. (a) Fit comparison between heterodyne (greed dashed) and CONTIN (red dashed) methods of PolyU intensity correlation (blue). Secondary y axis and dots report difference between fits and data. (b) Zoomed portion of panel (a) highlighting the poor exponential fit for polydispersed data. (c) CONTIN extracted R_h distributions for hard spheres (dark red), and corrected for unstructured polymers (light red). (d) CONTIN fit (dashed red), with the corresponding relaxation times distribution (solid red) and the average relaxation times given by heterodyne exponential fit. (e) Average hydrodynamic radius given by the CONTIN (red) and heterodyne fitting method. Shaded area report the producer specified size distributions. Black line show the R_h dependency from monomer number N for an ideal chain. Solid red line is the CONTIN polymer radius distribution plotted also in panel (c).

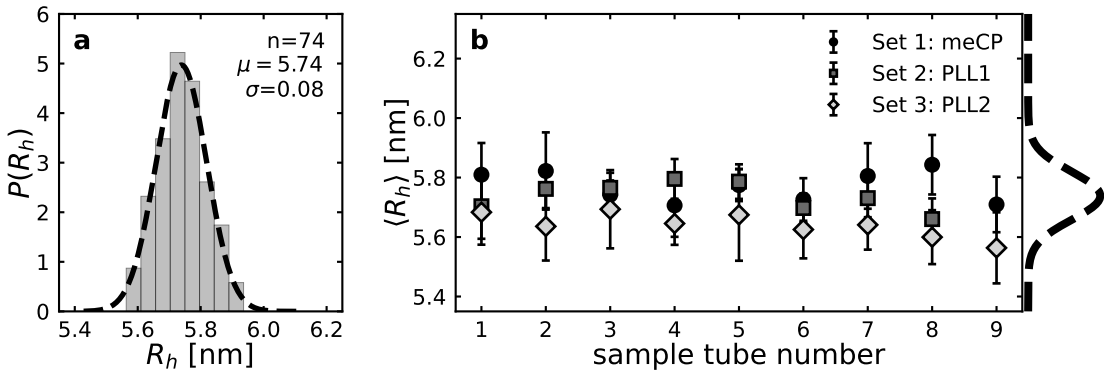

Figure S3: (a) Statistical distribution of n independent PolyU hydrodynamic measurements through DLS and heterodyne analysis, fitted with a Gaussian (black dashed curve in panel a and b) having $\mu = 5.74$nm and $\sigma = 0.08$ nm. (b) Comparison between average measured radii of sets of independent PolyU samples prior to the addition of peptides, subsequently used to study PolyU-peptide interaction.

To this aim, we analyzed the $g_2(\tau)$ correlation functions using the CONTIN algorithm [14, 15], as implemented in the data analysis routine of a LSI Correlator (v3.2.5, LS Instruments AG, Switzerland). Through CONTIN analysis we were able to estimate the distribution in coil hydrodynamic radius and therefore the monomer length distribution of the PolyU samples.

The outcome of CONTIN, however, needs to be adjusted. The contribution to the scattered electric field correlation function of each scatterer with $R_h \ll \lambda$ is proportional to its squared mass. CONTIN is built around the notion that such contribution is proportional to ${R_h}^6$ as in the classic treatment of polydispersed spherical scatterers [16]. This assumption is however inadequate for random coils where, instead, the mass of each chain grows with ${R_h}^2$ so that the contributions to the field correlation function is proportional to ${R_h}^4$. Thus, to extract from CONTIN the distribution probability $P^P(R_h)$ of polymers of hydrodunamic radius R_h, we need to correct the correlator-computed CONTIN distribution $P^C(R_h)$ by weighting each section of the distribution by ${R_h}^2$, which leads to:

$$P^P(R_h) \propto P^C(R_h){R_h}^2 \tag{S8}$$

$P^P(R_h)$ and $P^C(R_h)$ are plotted, after normalization, in Fig. S2c after implementing a correction of 1.32, from the effect of the heterodyne component to the intensity autocorrelation, as discussed above. Red dashed line and red shading are $\langle R_h^P \rangle$, and $\sigma_{R_h^P}$ respectively. The corresponding distribution in relaxation times $P^P(\tau)$ that contribute to $g_2(\tau)$ are shown in Fig. S2d.

The accuracy in the measurement of R_h is reported in Fig. S3a, where we show the normalized distribution in values of the hydrodynamic radius of PolyU before adding peptides extracted with the exponential heterodyne method from intensity correlation functions having duration of 2000 seconds. The distribution is well approximated by a Gaussian (dashed lines in panel a and on the right hand

side of panel b). We obtain a standard deviation of 0.08 nm. In panel S3b we plot R_h measured in the three sets of 9 samples each of PolyU before the addition of cationic peptides. Set 1, 2 and 3 were employed for the study of PolyU-meCP, PolyU-PLL15 and PolyU-PLL45 phase separation, respectively. The three sets have minor systematic differences that we attribute to RNA shortening due to degradation and/or minor differences in the optical alignment. The difference between sets is however comparable to the standard deviation.

S4 Thermal stability of pre-transitional complexes and phase transition

To investigate the energetic contribution of the PolyU-peptide interaction, discussed in greater detail in section S8.1, we examined the thermal stability of the phase separation process analyzing two components: the pre-transitional soluble complexes and the dense phase yield at fixed sample composition q^+/q^-.

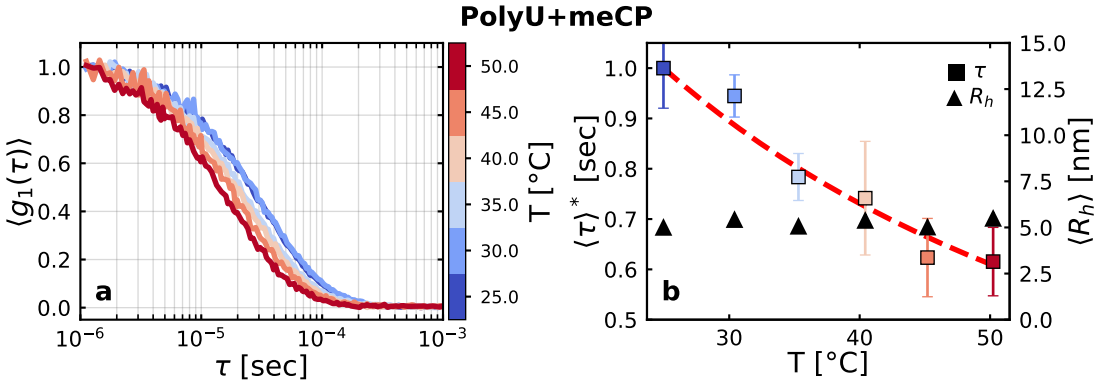

Figure S4: Temperature scan of DLS measurements of PolyU and meCP peptides prepared at charge ratio $q^+/q^- \approx 0.15$. Panel (a) reports the average $g_1(\tau)$ correlation functions acquired in a 25-50 °C temperature range. Panel (b) presents the corresponding normalized fitted relaxation times ($\langle\tau\rangle^*$ colored squares, left axis) and extracted hydrodynamic radius ($\langle R_h\rangle$ black triangles, right axis). The red dashed line corresponds to the normalized water viscosity η dependence on temperature. Relaxation times trend does not deviate significantly from water viscosity, indicating the independence of PolyU coil radius from the temperature in the explored range.

For the individually dispersed PolyU-peptide soluble complexes, light scattering measurements were performed on a PolyU-meCP sample prepared at $q^+/q^- \approx 0.15$, a composition outside the instability region of the phase diagram, where no dense phase is formed (Fig. S4). DLS data revealed a smaller radius compared to pure PolyU samples, consistent with peptide binding to RNA coils. The measured radius remained constant within the explored temperature range (25-50 °C), and the observed decrease in the relaxation times of the correlation functions is solely due to the variation in solvent viscosity with temperature. No detectable T dependence is thus observed.

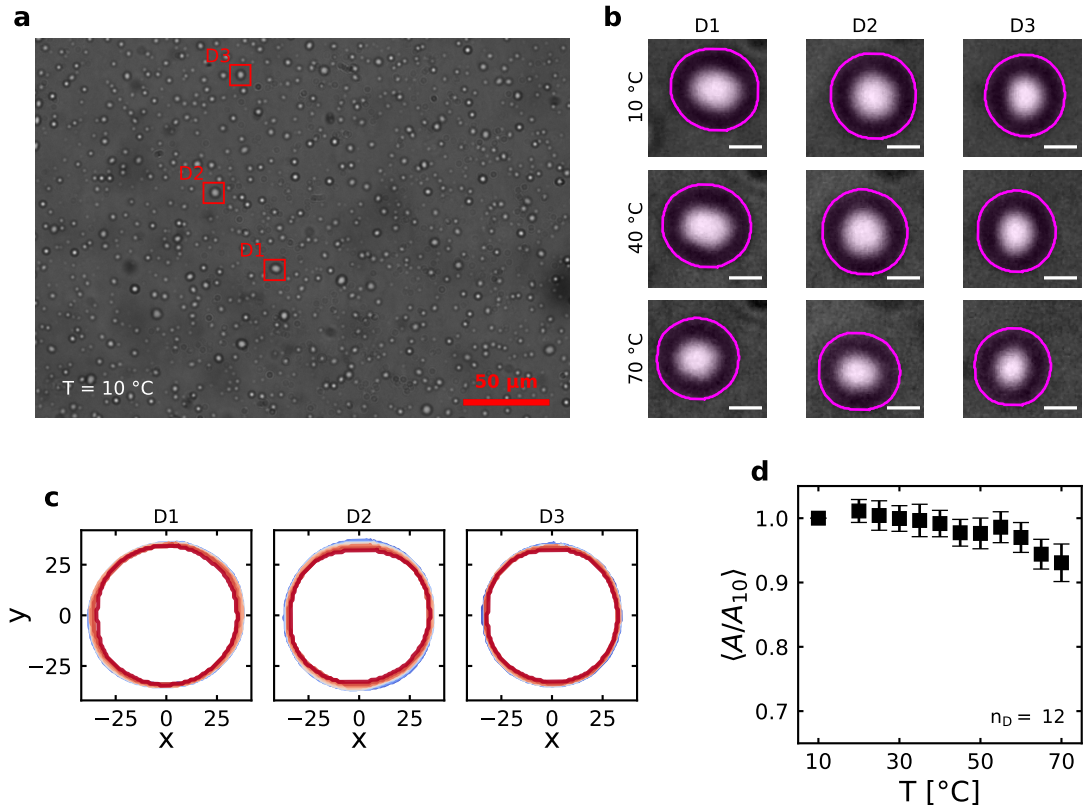

Figure S5: Thermal stability of dense phase droplets. (a) Brighfiled image image of full field of view of the the dense phase droplets. $n_D = 12$ significative droplets were chosen, individually segmented (panel b, scalebars equivalent to 3 μm), and their profiles were extracted (panel c) in order to retrieve the relative change in surface area of the droplets varying the sample temperature (panel d).

To study the phase separation yield as a function of T, dense phase droplets formed in a sample of PolyU-meCP prepared at $q^+/q^- \approx 0.5$ were deposited on a microscopy glass slide coated with a 3 wt% Bovine Serum Albumin solution (Fig. S5). Sample composition was chosen to yield a RNA dense phase sedimentation involving a fraction $n_s/n \approx 0.5$ of PolyU chains, as determined from SLS data (see Fig. 2 of the main text). Individual droplets were segmented, and their profiles were determined for each tested temperature between 10 °C and 70 °C. This analysis allowed us to quantify the surface area occupied by each droplet and to measure its relative variation in temperature. Data show a slight decrease in phase separation, nearly negligible up to 50°C, and more pronounced at larger T. This mild T dependence enables giving an upper estimate to the possible difference in binding enthalpy between dilute and dense phase, ad discussed in section S8.1,

S5 Derived quantities

For each sample, known quantities are:

- V, the total sample volume
- n and p, respectively the total number of moles in the system for RNA chains and peptides, derived from the mixing concentrations as $n = c_{RNA}V$ and $p = c_pV$

From scattering experiments, both dynamic and static, the direct observables extracted as a function of the charge ratio or of the stoichiometric ratio of the system are (Fig. S6):

- R_{g0} and R_g, the gyration radius of the RNA coils in solution before and after the addition of peptides.
- $\langle I\rangle_0$ and $\langle I\rangle$, the mean scattering intensity for pure PolyU samples ($p = 0$) and PolyU-peptides mixtures in solution ($p/n > 0$)

The knowledge of these quantities enable a quantitative determination of several parameters that describe the phase behavior of the system. Since $\langle I\rangle_0 \propto c_{RNA}$ and $\langle I\rangle \propto c_{RNA,s}$ as explained in sections S2.1 and S3.1, the fraction n_s of PolyU that remains in solution is given by

$$n_s = n\frac{\langle I\rangle}{\langle I\rangle_0} \tag{S9}$$

The fraction that demixes into the dense phase is thus $n_d = n - n_s$. Assuming that all peptides are bound to an RNA chain (see section S7.1), it is possible to estimate the effect on the coil shrinking obtained with the binding of each peptide. This is achieved extracting the linear slope of the $R_g\, vs.\kappa_s$ by fitting radius data in the first regime where the system is still homogeneous $R_g = R_{g0}(1 - \alpha_\kappa\, p/n)$. The same behavior can be expressed using an analogous coefficient α_q if the concentration of peptides is expressed as a function of the number of positive charge they carry. The linear dependence of R_g on κ_s changes slope when considering the radii measured in the dilute phase after the transition (phase III). To obtain an estimate of the degree of peptide decoration of the solubilized chains in phase III we exploit the linear behavior observed in phase I. Accordingly, we assume that the stoichiometric ratio

$$p_s/n_s = \kappa_s = \left(1 - \frac{R_g}{R_{g0}}\right)/\alpha_\kappa \tag{S10}$$

is related to the radius R_g in the same way in phase III as in phase I. This corresponds to the projection drawn in Fig. S6 through the red construction. As explained in the main text and in Section 6.2 below, this assumption is equivalent to say that the type/size of tangles that PolyU forms around each peptide is a local phenomenon that cannot be influenced by remote molecular clustering and thus is the same in phase I and III.

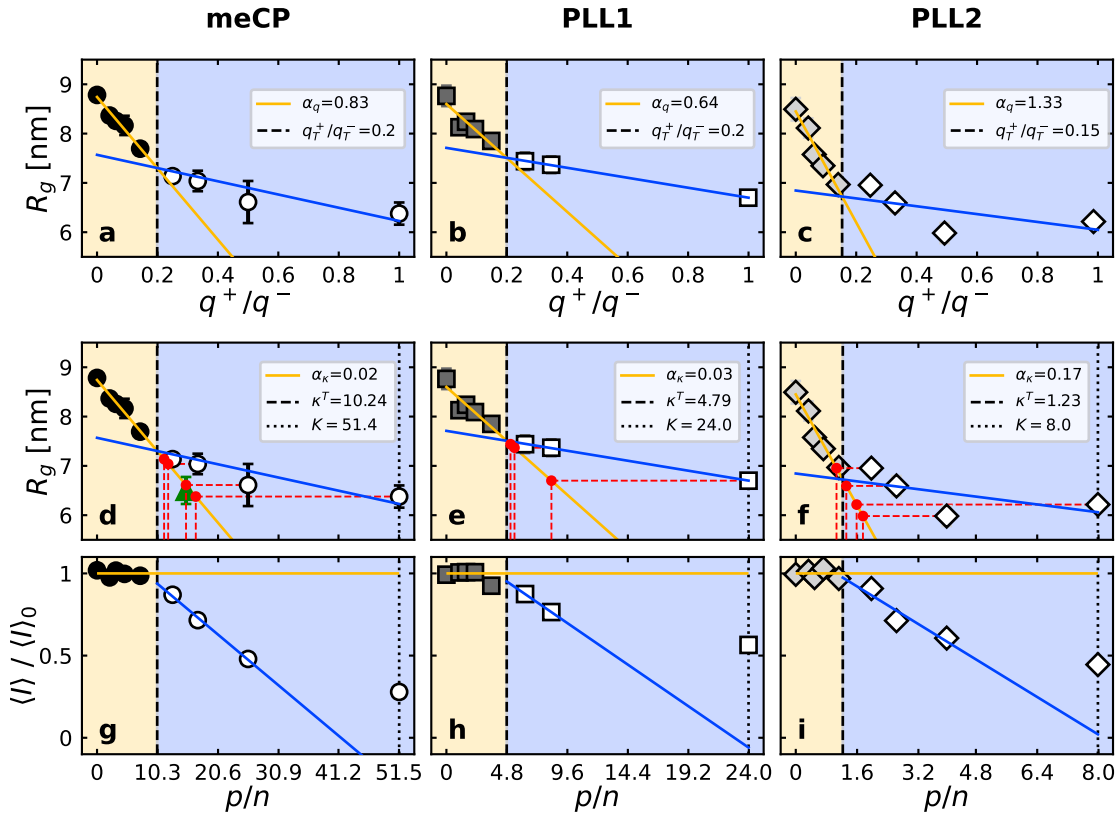

Figure S6: Experimental data extracted from static and dynamic light scattering measurements for mixtures of PolyU and each of the three different peptides (columns) across the phase transition for homogeneous (yellow shading) or demixed (blue shading) samples. Top row (panels a-c) shows gyration radius of the PolyU coils as a function of the system charge ratio q^+/q^-. Yellow solid line shows the linear fit for the radius data in the single phase regime from which the coil shrinking rate per bound positive charge α_q is extracted. Dashed black line indicates the threshold charge ratio q_T^+/q_T^-. Middle (panels d-f) and bottom (panels g-i) rows report respectively the radius and relative intensity data as a function of the stoichiometric ratio of the system p/n. In panels d-f are shown: fit for the radius data in homogeneous sample (yellow solid line) having the compaction coefficient per bound peptide α_κ, stoichiometric ratio at the phase separation threshold κ^T (black dashed line), maximum number of peptides that can bind a single PolyU chain $K = Q_n/Q_p$ (dotted black line). In red are reported the projection of the R_g data for demixed samples on the fit of R_g for the homogeneous regime, used to extract the stoichiometric ratio k_s of the soluble RNA-peptide complexes after phase separation. The green marker in panel d report the measured gyration radius of a sample having initial RNA concentration about half of the samples of the main set of measurements, and a peptide concentration computed in order to obtain the stoichiometric ratio p/n given by the projection of the sample having $q^+/q^- = 0.5$ on the linear fit for the radius data in homogeneous sample, as further explained in section S6.

The knowledge of p_s/n_s enables determining the number of peptides in the dense phase ($p_d = p - p_s$), as well as the average number of peptides bound to each RNA chain in the dense phase $\kappa_d = p_d/n_d$. The values of molecular composition for both phases extracted from experimental data are represented in Fig. 6 of the main text for all three peptides, expressed as fraction of RNA chains in the dilute phase, and number of peptides per RNA over the maximum amount of peptides that can bind each chain.

For meCP peptide, confocal microscopy experiments allowed to have a direct access also to the volume fractions of the dense phase ϕ_d for demixed samples. Combining the information of the dense phase volumes $V_d = \phi_d V$ with the moles of both species in the two phases, we can compute the concentrations of the dense and dilute phase. The results are shown in Figure 3.d-e of the main text.

S6 Further measurements confirming the linear R_g *vs.* p/n dependence

To better understand and confirm the linear scaling of the measured PolyU gyration radius decrease with peptide addition in the homogeneous (II) phase, we performed a supplementary set of measurements, producing four new samples (Fig S7).

The first two were designed to reproduce the behavior of the sample prepared with a PolyU-meCP mixture having charge ratio $q^+/q^- = 0.5 \approx p/n = 25.7$, which relative scattering intensity and gyration radius are plotted in Fig 2c-d of the main text and reported in Fig. S7. Performing scattering measurements of the surnatant (phase III) after equilibration and centrifugation of the sample to sediment the dense phase, we observed, confirming the results presented in the main text, phase separation upon the addition of peptides in the PolyU solution, with a decrease in the scattered intensity $\langle I \rangle / \langle I_0 \rangle \approx 0.45$, a value close to $\langle I \rangle / \langle I_0 \rangle \approx 0.48$ observed in the main set of experiments. DLS measurements, similarly, showed a compacted RNA gyration radius $R_g(q^+/q^- = 0.5) \approx 6.33$ nm, matching what found in the main set of measurement were $R_g(q^+/q^- = 0.5) \approx 6.61$ nm. Following the procedure presented in section S5 we could estimate from the reduced radius and intensity the stoichiometric ratio of the dilute phase as $\kappa_s \approx 16.2$.

In parallel we produced a second pair of samples, one of which prepared to lay on the phase boundary of the dilute phase observed in the sample described above. Accordingly we prepared a PolyU-meCP mixture with an initial RNA concentration $c_{RNA} = 13.5\,(\langle I \rangle / \langle I_0 \rangle) = 13.5 \cdot 0.45 \approx 6\ \mu$M and a stoichiometric ratio $p/n = 16.2$. Without observing any phase separation, we obtained both a relative scattering intensity $\langle I \rangle / \langle I_0 \rangle \approx 0.46$ and a gyration radius $R_g \approx 6.46$ nm similar to the dilute phase of the demixed sample. The obtained radius is found to lay on the extrapolation of the linear fit for data in phase II at values of p/n above the phase transition threshold, a behavior that we use to build the construction that allow us to estimate stoichiometric ratios in the dilute phase.

These results enabled us to explore the radius reduction in the homogeneous

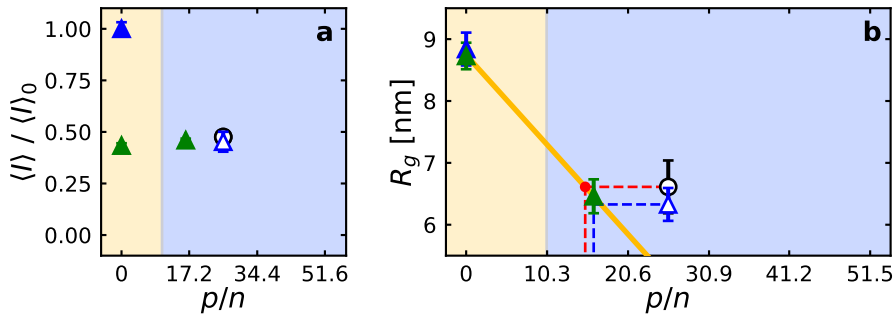

Figure S7: Measurements supporting the linear scaling of R_g *vs.* p/n. (a) Average scattered light intensity $\langle I \rangle$ normalized to the initial scattering intensity $\langle I \rangle_0$ of PolyU only and (b) measured gyration radius of the PolyU in the homoegneous (II) or dilute (III) phase in the demixed samples. Empty black circles report the value of $\langle I \rangle / \langle I_0 \rangle$ and of R_g for the dilute phase of PolyU-meCP sample prepared at $q^+/q^- = 0.5$, also plotted in Fig 2c-d of the main text. Red dot shows the estimated dilute phase stoichiometric ratio κ_s obtained with the red construction using the linear fit of the radii in the homogeneous regime (yellow solid line). Blue triangles mark the measured relative intensity and radius values for PolyU before the addition of peptide ($p/n = 0$, filled blue marker), and for the dilute phase after peptide addition and demixing ($q^+/q^- = 0.5$, empty blue marker). Green filled triangles report the relative intensity and R_g of a PolyU solutions at concentration about half of what considered in the data of the main text. This samples were prepared without ($p/n = 0$) and with meCP, the latter at a concentration chosen to have a stoichiometric ratio p/n matching the one found in the dilute phase of the demixed sample, obtained from the projection on the linear fit (dashed blue lines) in panel b of the empty blue markers.

phase for p/n values not accessible with the original concentrations adopted in the main set of experiments, confirming that at these increased values of p/n the radius reduction remain linear with the peptide addition and further supporting the reliability of our estimate of κ_s. Moreover, these data also confirm that the bend in the observed dependency of R_g *vs.* p/n observed at the phase transition is due to the uneven partitioning of the peptides induced by demixing, without which there would not be any bending.

S7 Model Setting

Our observations indicate that the LLPS is located at an intermediate p/n, corresponding to $q_T^+/q_T^- = q^+/q^- \approx 0.2$, a value much smaller than the charge balance. One of the central aims of this paper is to investigate what controls the position of the phase transition. We thus developed a simple model in which we determine the phase transition on the basis of the other experimental observations:

- the radius of solubilized chains shrinks with the number of peptides per PolyU molecule κ_s, where $\kappa_s = p/n$ for $q^+/q^- < q_T^+/q_T^-$;

- the PolyU concentration in the dense phase is approximately constant;
- peptides unevenly partition between the two phases, with a higher number of peptides per RNA chain in the dense phase $\kappa_d > \kappa_s$;
- PolyU chains in the dense phase are fluid.

In this section, we list the factors that play or could play a role in the condensation and phase transition, and describe how we include them in the model.

S7.1 Interactions between peptides and nucleic acids

In solution, positively charged peptides bind to negatively charged PolyU. The free energy of binding can be attributed to electrostatic interactions, with the main contribution coming from the entropy gained by the released monovalent counterions [17, 18] and to electrostatic entropy [19].

Experiments on the interaction thermodynamics between oligolysines and PolyU RNA [17] show that at the ionic strength conditions that we tested and for our poly-lysine cationic valence, the dissociation equilibrium constant is one order of magnitude smaller than the lowest peptide concentration used in the scattering experiments. These data support the assumption that throughout all the experiments and model development nearly all peptides are always bound to RNA chains, either in the dilute phase or in the dense phase.

The peptide-PolyU interactions mediate PolyU-PolyU interactions, which can be either intra-chain, yielding coil compaction (see section S7.2), or inter-chain, resulting in the formation of the condensate. The range of peptide-mediated PolyU-PolyU interactions is determined by the screening length λ_D and by the mean size of the peptides. The former, $\lambda_D \approx 7$ Å, is much shorter than the PolyU size. The size of the two shortest peptides considered in this work can also be safely considered much smaller than the PolyU coils, having mean radii of about 1.5 nm [20, 21].

We indicate with $\delta\varepsilon = \delta h - T\delta s$ the free energy associated to the binding of each peptide to a PolyU chain. δh_s and δh_d are the binding enthalpy of a single peptide to individually solubilized PolyU and to PolyU in the dense phase, respectively. Analogous definition for δs_s and δs_d. We also define $\Delta\varepsilon = \delta\varepsilon_d - \delta\varepsilon_s$, $\Delta h = \delta h_d - \delta h_s$ and $\Delta s = \delta s_d - \delta s_s$. These quantities do not include contributions from the conformation entropy of PolyU, which will be evaluated below, but may include contributions such as effects due to the conformational entropy of the peptides or due to salt partitioning between phases. The small size of the peptide-PolyU - and thus PolyU-PolyU - binding sites with respect to PolyU coils suggests that the peptide-PolyU binding strength cannot depend significantly on the phase the PolyU is in, since the two local environments are basically indistinguishable. However, we keep them as parameter in the model.

By analyzing the observations with the use of our model, we will obtain quantitative estimates of these quantities

S7.2 Entropy reduction associated to the compaction of RNA chains

As PolyU chains dispersed in the solution become decorated by peptides, their radius R_g shrinks from the unperturbed R_{g0} (Fig. 5 panel b of the main text). Such reduction comes from the formation of peptide-mediated intra-chain bonds. Experiment show that such reduction, in the weak decoration range, is linear in the number of peptides:

$$R_g(\kappa_s) = R_{g0}(1 - \alpha_\kappa \kappa_s) = R_{g0}\left(1 - \alpha_q \frac{q^+}{q^-}\right) \tag{S11}$$

The linear decrease of R_g implies an effect on the PolyU coil proportional to the number of peptides decorating the RNA chains. This observation, combined with the fact that all peptides are bound, suggests that around each peptide-PolyU bond the two chain form a compact complex in which they are tangled. Since the portions of PolyU involved in such complexes cannot adopt open conformations, they do not contribute to the coil radius. In other words, the PolyU behaves as if its contour length were reduced from L_0 to an effective length $L(\kappa_s) = L_0 - \kappa_s \ell$, where ℓ is a parameter to be determined from observations. This effective shortening of the contour length is described in the sketch in Fig. S8a, where the effective length is obtained connecting the polymer ends through the shortest path, jumping across loops on the pinching sites.

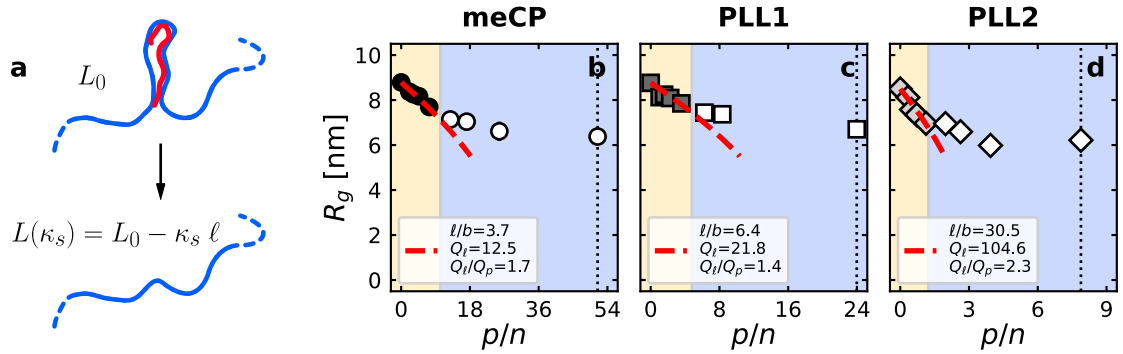

Figure S8: (a) Schematic drawing of the contour length reduction used to compute the length of RNA chain ℓ involved in each peptide mediated loop. In blue is shown the PolyU chain, while the peptide is represented in red. L_0 is the initial and total contour length of the RNA chain, $L(\kappa_s)$ is the effectively reduced contour length obtained by removing loops as the one sketched here. (b-d) Reduction of the gyration radius as a function of the average number κ of peptides per PolyU for the three different peptides used in the experiments. Symbols: experiments. Dotted like: stoichiometric ratio p/n at which $q^+/q^- = 1$. Dashed curve: best fit of the dark points obtained by assuming that each peptide brings about a reduction of the PolyU length of ℓ/b Kuhn segments. Q_ℓ is the average number of PolyU monomers and thus of negative charges involved in each peptide-mediated loop. The parameter Q_ℓ/Q_p indicates the charge ratio in each loop, with Q_p being the positive charged present on each peptide

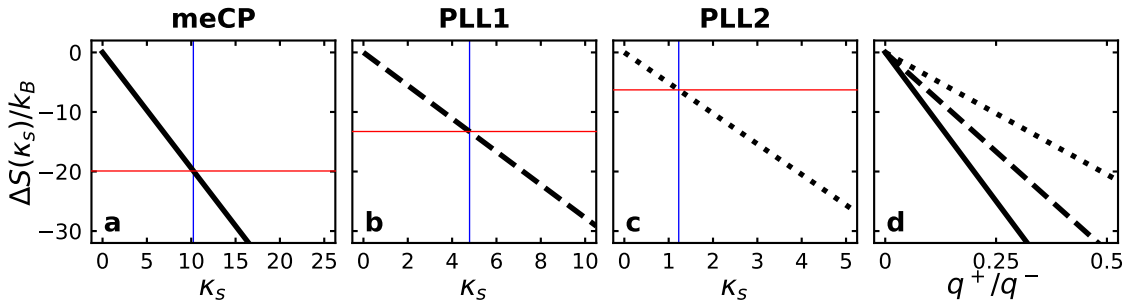

Figure S9: (a-c) Black line, entropic loss of PolyU gyration radius reduction due to loop formation as a function of number of peptides per RNA chain (κ_s). Blue line mark the peptide per RNA ratio of the phase separation threshold κ^T. Red line mark the PolyU chain entropy loss ΔS_T at the point of phase transition $\kappa_s = \kappa_T$. (d) Entropic loss of radius reduction as a function of the overall system charge ratio. Notice that the entropic cost of PolyU compaction at equal peptide charge is larger for the smallest peptide. This is because the conformational reduction is larger when forming a larger number of smaller loops than a smaller number of larger loops.

The effectively reduced coil length $L(\kappa_s)$ contains $N_b - (\kappa_s\,\ell/b)$ Kuhn segments. As a consequence, its gyration radius according is:

$$R_g(\kappa_s) = b\,(N_b - \kappa_s\,\ell/b)^{1/2}\,6^{-1/2} \tag{S12}$$

It is possible to estimate ℓ/b by searching for the best fit of this expression to the experimental $R_g(\kappa_s)$ (Fig. S8b-d). We find: $\ell/b \approx 3.7$ for meCP, $\ell/b \approx 6.4$ for PLL15, $\ell/b \approx 30.5$ for PLL45. Expressed in number of PolyU charges involved in the loop we obtain (using $\xi_p = 1.1$ nm) $Q_\ell \approx 12.5$ for meCP, $Q_\ell \approx 21.8$ for PLL15, $Q_\ell \approx 104.6$ for PLL45, indicating that the loops comprise a PolyU/peptide charge ratio of about $Q_\ell/Q_p = 1.4 - 2.3$.

The formation of local peptide-PolyU dense complexes certainly reduces the conformational space accessible to the PolyU chain. To quantify such chain entropy loss, we adopted the simple approach of considering such complexes as loops of average length ℓ. Within this framework, the entropy loss is proportional to the number of peptides bound to the chain $\Delta S(\kappa_s) = S(\kappa_s) - S_0 = \kappa_s\,\delta S_\ell$ where S_0 and $S(\kappa_s)$ are the entropy of the PolyU coil in solution in the absence and presence of κ_s bound peptides, respectively, and δS_ℓ is the entropy loss due to the formation of a single loop of length ℓ. δS_ℓ can be evaluated following standard approaches based on the probability of end-to-end contact in a chain of length ℓ and same Kuhn length b as the PolyU [22, 23, 24]. Indeed, the ratio of the number of polymer conformations with an end-to-end distance r to the total number of conformations, is given by the distribution $P(r)$ of the end-to-end distance

$$P(r) = \left(\frac{3}{2\,\pi\,b\,\ell}\right)^{3/2} exp\left(-\frac{3r^2}{2\,b\,\ell}\right) \tag{S13}$$

so that the fraction of conformations in which $r < \delta r$ is

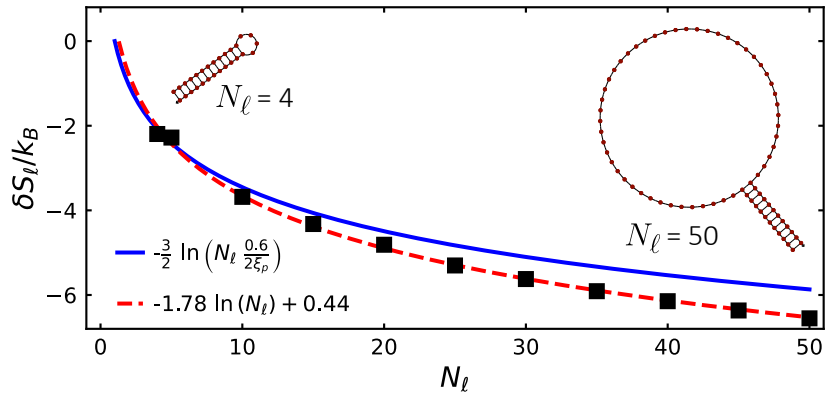

Figure S10: Entropy variation upon ssRNA loop formation. Blue line represent the increasing entropic loss increassing the loop length expressed in number of monomers according to equation S16, in which 0.6 is the inter-monomer distance. Black dots have been computed using Nupack [25] retrieving the secondary structure free energy of RNA strands having sequence 5'-GCGCUUAAGCGC-{U}$_{N_\ell}$-GCGCUUAAGCGC-3', forming loops of increasing length N_ℓ and fixed stem length. Examples of the structures used for N_ℓ =4 and 50 are shown in the picture.

$$P(|r| < \delta r) = \sqrt{\frac{6}{\pi}} \left(\frac{\delta r}{\ell}\right)^3 \left(\frac{\ell}{b}\right)^{-3/2} \tag{S14}$$

from which

$$\delta S_\ell = \log\left[\sqrt{\frac{6}{\pi}} \left(\frac{\delta r}{b}\right)^3\right] - \frac{3}{2}\log(\ell/b) \tag{S15}$$

Here and in the following entropy is expressed in units of Boltzmann constant k_B.

An estimate of the value of δr - the distance at which the two terminals of the loop are kept from each other - is conveyed by the way in which ℓ is determined from the experiments. Since we effectively subtract ℓ from the contour length, we imply that the terminals of the loop are at about a monomer distance. This means that the quantity in squared parenthesis has a value close to 1. We are thus just left with

$$\Delta S(\kappa_s) = \kappa_s\, \delta S_\ell \approx -\kappa_s\, \frac{3}{2}\, \ln(\ell/b) \tag{S16}$$

Fig. S9 shows the decrease of $\Delta S(\kappa_s)/k_B$ as peptides bind the PolyU chain computed from the values of ℓ determined from the experiments for the three different peptides (see Fig. S8). We can notice that $-\Delta S(\kappa_s)$ is largest for the smallest peptides, in agreement with the larger entropic cost of many smaller loops *vs.* few larger loops. For the discussion below it is useful to introduce ΔS_T as the entropy cost due to loop formation at the phase transition point. In the case of meCP, $\Delta S_T \approx -20$.

To strengthen our estimate of δS_ℓ, we compared it with entropy values obtained using RNA free energy calculators based on experimental database [25]. Figure S10 shows the entropy penalty of forming a loop involving N_ℓ monomers as derived from the Nucleic Acid Package (NUPACK) software together with the same penalty computed according to equation S16. The former results from the free energy calculation of a stem-loop structure in which we kept the stem length fixed and increased the number of monomers in the loop. We find that NUPACK entropy variations depend on the logarithm of the loop length N_ℓ, as expected and in agreement with our estimate, varying only slightly from the one we adopted. This comparison confirms our value for δS_ℓ that is, if anything, underestimating the free energy cost of the loops.

Overall, the experimental finding that ℓ grows linearly with the cationic charge of the peptides with a small proportionality coefficient ($1 < Q_\ell/Q_p < 2.5$), supports the notion that the effect of peptides is to form complexes and agrees the notion that to minimize entropic penalty loops shrink to their minimum length.

S7.3 Entropy from demixing

The formation of the dense phase also corresponds to a lowering of the translational freedom of the PolyU, which is of the order of $\Delta S_{CM} = S_{CM,0} - S_{CM,d} = k_B \ln(\rho_d/\rho_0)$, where $\rho_0 = n\, m_{PolyU}/V$ and $\rho_d = (n - n_s)\, m_{PolyU}/V_d$ are the densities of PolyU in the dilute and dense phase, respectively. V_d indicates the volume filled by the dense phase.

S7.4 Entropy of the RNA chains in the dense phase

The PolyU that collapse in the dense phase modify their entropic state. In the dense phase a fraction of the peptide can form inter-chain complexes across different RNA coils. The availability of inter-chain contact enable PolyU chains in the coacervate to expand through interpenetration (Fig. 5c of the main text), as also indicated by DLS evidence of reversible entanglement. We have no experimental access to the entropy S_d of PolyU in the dense phase, difficult also to quantify due to the possibility of peptides in the dense phase to give rise to intra-chain contacts reducing coil entropy and to inter-chain contacts favouring conformational relaxation, in the model we introduce $\Delta S_d = S_d - S_0$. The nearly constant density of such phase as peptides are added, suggests that $\Delta S_d = S_d - S_0$ can be assumed to be a constant quantity, independent from p/n. We expect that $S_d < S_0$.

S7.5 Entropy associated to the distribution of peptides among PolyU

As the dense phase is formed, the system becomes non-homogeneous, with peptides partitioning unevenly between the two coexisting phases, so that the mean number of peptides per PolyU chain in the dense phase is different from the one in the dilute phase $\kappa_d \neq \kappa_s$. Such partitioning lowers the number of possible peptide-PolyU

distributions, corresponding to a loss of entropy with respect to the condition of maximum which would be given by a uniform distribution of peptides among PolyU molecules. To estimate this quantity in the model below we assume that each PolyU can host up to a maximum K of bound peptides that we have set to correspond to the charge balance (the total cations in K peptides equals the total anions in a single PolyU, $KQ_p = Q_{RNA}$). Accordingly, the number of ways the κ_d and κ_s peptides can locate on the RNA chains is given by the binomial coefficients $\binom{K}{\kappa_d}$ and $\binom{K}{\kappa_s}$, respectively.

S8 Theoretical model

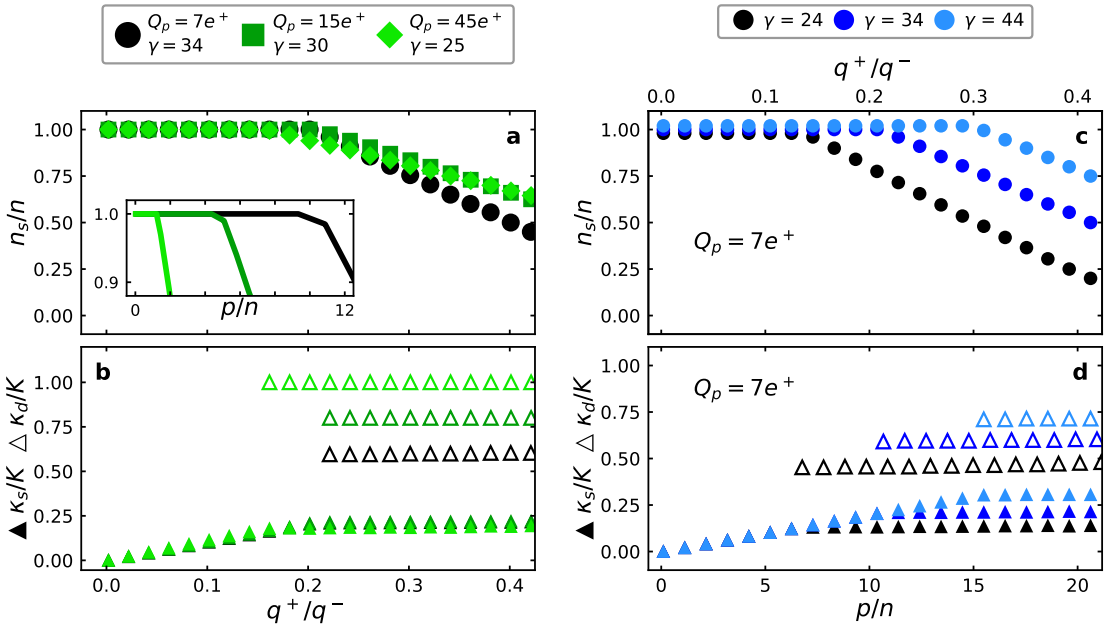

Figure S11: Results of the theoretical model. (a-b) Results for the fraction of RNA chains in solution (a) and the fraction of peptides over the maximum number of peptides that can be bound to each RNA chain in both phases (b). The different values of Q_p are chosen to match the charges on the different peptide species. For each of them the parameter γ was chosen to match the experimentally observed phase transition. The inset in panel a shows the fraction of RNA chains in solution n_s/n as a function of the stoichiometric ratio in the system p/n, highlighting the difference in threshold position expressed in peptide per RNA chain. (c-d) Results for the fraction of RNA chains in solution (c) fraction of peptides over the maximum number of peptides that can be bound to each RNA chain in both phases (d) for a choice of $Q_p = 7$ e$^+$ varying γ. Slight variations of this parameter shift significantly the predicted phase separation boundary.

We consider a solution containing n PolyU within a volume V. In this solution, we introduce p peptides. When a peptide is injected, it will attach to an RNA chain. The model is built under the assumption that the solution is in general split between

the dilute and dense phase, each defined by key features observed in the experiment. In the dilute phase, PolyU chains undergo the observed compaction indicating a reduced conformational entropy. In the dense phase, PolyU are entangled at a concentration that does not depend on the volume fraction of the phase, nor on p. In the model, the quantities to be determined from a minimization of the free energy are:

- n_s, the number of PolyU individually dispersed in the dilute phase, corresponding to a fraction $\Psi = n_s/n$ over the total number n of chains. $n_d = n - n_s$ is the number of RNA chains in the dense phase.

- $\kappa_s,\ \kappa_d \in [1, K]$ the average number of peptides per PolyU, in the dilute and dense phase, respectively. Since peptides are either attached to individually dispersed or condensed PolyU, calling $\kappa_{s,i}$ and $\kappa_{d,j}$ the number of peptides decorating the i-th and j-th RNA chain in the dilute and dense phase, respectively, we obtain
$$\sum_{i=1}^{n_s} \kappa_{s,i} + \sum_{i=j}^{n_d} \kappa_{d,j} = \kappa_s\, n_s + n_d\, \kappa_d = p \tag{S17}$$

On this basis we construct the partition function by considering all the possible choices of partitioning of PolyU between the two phases and, given that, all the possible choices of peptide distribution on the RNA chains. We thus choose n_s PolyU among the n available, free to move in the volume $V - V_d$, where V_d is the volume of the dense phase. Each of these states is weighted with the Boltzmann factor depending on the entropies and energies of the two phases, as discussed above.

$$\begin{aligned}\mathcal{Z}(n,p) = &\frac{1}{n!}\sum_{n_s=0}^{n}(V-V_d)^{n_s}V_d^{n_d}\binom{n}{n_s}\\ &\sum_{\{\kappa_s,\kappa_d\}}\prod_{i=1}^{n_s}\binom{K}{\kappa_{s,i}}\prod_{j=1}^{n_d}\binom{K}{\kappa_{d,j}}e^{\sum_{i=1}^{n_s}(\Delta S(\kappa_{s,i})-\beta\kappa_{s,i}\delta\varepsilon_s)+\sum_{j=1}^{n_d}(\Delta S_d-\beta\kappa_{d,j}\delta\varepsilon_d)},\end{aligned} \tag{S18}$$

where the summation $\sum_{\{\kappa_s,\kappa_d\}}$ is over all possible $\kappa_{s,i}$, $i = 1, \ldots, n_s$ and $\kappa_{d,j}$, $j = 1, \ldots, n_d$ such that $\sum_{i=1}^{n_s}\kappa_{s,i} + \sum_{j=1}^{n_d}\kappa_{d,j} = p$. We thus need to minimize the free energy $F = -\ln \mathcal{Z}(n,p)/n$ with respect to Ψ, $\kappa_{s,i}$ and $\kappa_{d,j}$. By adopting conventional approximations we obtain

$$\begin{aligned}\beta F(\Psi,\kappa_d) = &-\Psi\ln\left[1-\frac{\rho_0}{\rho_a}(1-\Psi)\right]\\ &+\Psi\ln\Psi-\Psi\Delta S(\kappa_s)+\Psi\left[\kappa_s\ln\kappa_s+(K-\kappa_s)\ln(K-\kappa_s)\right]\\ &+(1-\Psi)\left[\kappa_d\ln\kappa_d+(K-\kappa_d)\ln(K-\kappa_d)\right]-\gamma\Psi\end{aligned} \tag{S19}$$

where

$$\gamma = -\ln\frac{\rho_0}{\rho_d} - \Delta S_d + \frac{K}{2}\left(\frac{\Delta h}{T} - \Delta s\right) \tag{S20}$$

and

$$\kappa_s = \frac{p/n - \kappa_d(1-\Psi)}{\Psi} \tag{S21}$$

The expression above includes the notion that the summation over the different $\kappa_{s,i}$ and $\kappa_{d,j}$ is dominated by their average values κ_s and κ_d. From the minimization of $F(\Psi, \kappa_d)$ over its variables we can determine the predicted location of the phase transition and the p dependence of n_s/n, κ_s and κ_d. This is shown in Fig. S11, in which we show (panels a and b) the expected behavior of these quantities computed using the parameters Q_p, K, ℓ, and α_κ relative to the three peptides and with a choice of γ so that the phase transition is located at the value of p/n where it is experimentally observed. Panels c and d show the effect on the predicted phase behavior obtained when γ is changed, computed for the case of meCP.

Two comments are in order: (1) to obtain transitions at the same charge ratio with the different peptides it is necessary to chose larger γ for smaller peptides. Since only a fraction of the total amount of peptides in the dense phase are involved in inter-PolyU bonds, many of the peptides still produce loops and thus the related entropic loss, which - as in the homogeneous phase - is larger for a large number of small lops *vs.* for a small number of large loops, (2) larger values of γ shift the transition to larger p/n values because they embody larger penalties for the formation of the dense phase, either because of a larger entropic penalty in the dense phase or because of a difference in the peptide-PolyU bond energy favoring the dispersed condition.

S8.1 Enthalpic contribution to phase separation

In order to study the enthalpic contribution to the observed phenomena, we investigated the thermal stability of phase separation studying the dense phase volume fraction dependence on temperature (see section S4). We measured the variation in surface area occupied by individual dense phase droplets in the 10-70 °C temperature range as a proxy of the fraction of chains sedimented in the condensate n_d/n, assuming the dense phase density constant. Experiments showed a mild dependency on temperature, indicating that the bond enthalpic difference across the two phases is small. This observation can be used to derive an upper limit value for the bond enthalpy Δh.

The observed variation in $\langle A/A_{25}\rangle$ of about 7% can be assumed to reflect a similar variation in the fraction of chains that remain in the dilute phase Ψ. We studied the variation in Ψ evaluated at $p/n = 20$ varying γ in the range $20 < \gamma < 50$ (Fig. S12b). Notice how an increase in γ moves the phase separation threshold toward larger p/n, thus decreasing the fraction of sedimented RNA chains for a fixed stoichiometry ratio disfavoring phase separation as will be further discussed

in section S8.2. The choice of $p/n = 20$ was dictated by the fact that PolyU-meCP samples used for microscopy analysis were prepared at such stoichiometry ratio, at which $\Psi \approx 0.5$. This agrees with the model where for $\gamma = 34$, $p/n = 20$, cationic valence $Q_p = 7e^+$ as meCP we indeed obtain $\Psi \approx 0.5$. We found that to obtain a variation in Ψ matching the one we observe by changing T, we can set an upper limit to γ variations in $\Delta\gamma < 1.2$ (Fig. S12c).

Since the only term in γ that depends on T is $(K/2)\Delta h/T$, we can derive Δh by $\Delta\gamma = (K/2)(\Delta h/T)(\Delta T/T)$, where $K_{meCP} = 51$ and $\Delta T/T = 0.2$. We obtain $(K/2)\Delta h < 6$, and thus $\Delta h/T < 0.24$. This last value should be compared with the free energy involved in each loop formation $\Delta S_\ell = 2$ for meCP, indicating that the enthalpic contribution to the phase transition is basically negligible.

S8.2 Free energy contributions to parameter γ

From the definition of γ in Eq. S20, we can thus extract, in the case of meCP experiments, the values of the entropy contributions that we left implicit. Specifically we have that

$$-\Delta S_d - \frac{K}{2}\Delta s = \gamma + \ln\frac{\rho_0}{\rho_d} - \frac{K}{2}\frac{\Delta h}{T} < 35 \tag{S22}$$

If to this value we subtract $-\Delta S_T$ we obtain an estimate of the entropy variation of each PolyU chain in going from the dilute to the dense phase at the phase transition point. We obtain

$$-\Delta S_d - \frac{K}{2}\Delta s + \Delta S_T < 15 \tag{S23}$$

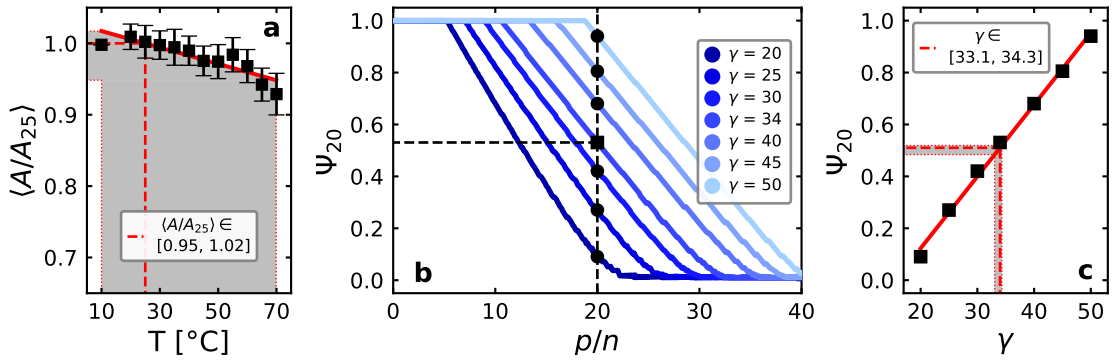

Figure S12: Study of the entalpic contribution to phase separation. (a) data from figure S5 showing a $\sim 7\%$ variation in the phase transition yield in the 10-70 °C temperature range. (b) Study of the phase transition yield expressed as Ψ computed at $p/n = 20$ for $20 < \gamma < 50$. For $\gamma = 34$ as used in the model for $Q_p = 6e^+$, $\Psi_{20} \approx 0.5$. Increasing γ decrease the phase transition yield, moving the transition threshold to larger p/n. (c) Mapping of a $\sim 7\%$ variation in phase transition yield experimentally measured to a variation $\gamma \in [33.1,\ 34.3]$.

The positive sign of this quantity indicates that the entropy of a chain in the dense phase is less than that in the dilute phase. The fact that at the transition chains collapse in the dense phase despite paying an entropy penalty indicates that there are other compensating factors contributing to the free energy. It is immediate to recognize that the entropy loss associated to collapsing is smaller than the entropy decrease that would result if the peptides that become bound to the collapsing phase were instead creating independent tangles in individually dispersed PolyU coils, *i.e.* $-\Delta S(\kappa_d) \gg -\Delta S_d - \frac{K}{2}\Delta s + \Delta S_T$.

A large part of the positive contribution to Eq. S23 could come from $\Delta S_d - \Delta S_T$, which contains the difference in conformational entropy between a PolyU chain in coexisting dilute (phase III of Fig. 1 of the main text) and dense (IV in Fig 1 of the main text) phase. This difference stems from two opposing terms: (1) the number of peptides per PolyU, larger in the dense phase, that could yield to an increased number of constrained tangled regions along the chain and (2) the conformational relaxation of PolyU chains through interpenetration demonstrated by the ergodicity observed by DLS in the dense phase. Further contributions could be conveyed by δs, the difference in the entropic component of peptide-PolyU binding between dilute and dense phase, a quantity that thus includes: effects due to the uneven partitioning of small ions in the dilute and dense phase - in turn modifying the entropy associated to counterion release in the two phases; effects related to the electrostatic entropy - due to the different composition and thus dielectric property of the two phases; effects due to structural difference between peptide-polyU bonds in which the bond connects two portions of the same chain (intra-chain bonds) or connects locations across chains (inter-chain bonds). Of this latter contribution δs contains only features that are not ascribable to PolyU chain conformations (which are taken care explicitly as discussed above) such as effects due to conformational difference of the peptide chain between inter-chain and intra-chain bonds.

Although we cannot safely disentangle these various contributions to Eq. S23, it can be appreciated that their combined effect is not large and it appears to oppose the phase separation. Altogether, the evidence and discussion offered in this work show that the conformational entropy penalty associated with the reduction of coil size that we unequivocally observe is enough to induce the phase separation. Thus should some of the factors listed above also favor coacervation, they would have to be included on top, and not in alternative, of the chain conformational effects here described.

Supplementary figures

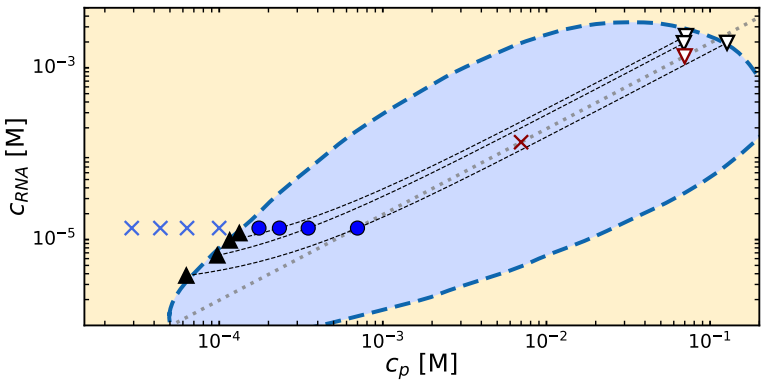

Figure S13: Experimental phase diagram in log-log scale reporting the initial solution composition (blue crosses for homogeneous samples, blue dots for demixed samples), dilute phase concentrations (black triangles) connected by tie-lines (dashed black lines) to corresponding dense phase concentrations (white downward triangle). Red markers represent the composition concentration and dense phase concentration of the sample described in Fig. 4 of the main text. Dotted gray line mark charge balance. The blue shaded instability region is drawn to guide the reader's eyes.

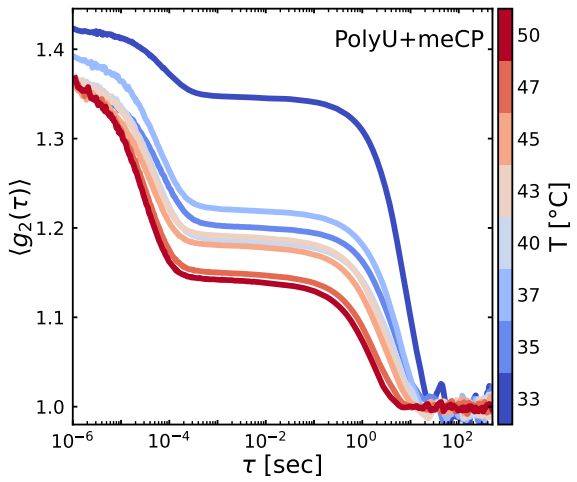

Figure S14: Raw average g_2 correlations from dynamic light scattering measurements of the condensate dense phase varying the sample temperature. It is relevant to note that $g_2(\tau = 0) \approx 1.42$, indicating that a Siegert value (see section S3.2) $\beta_0 \approx 0.42$, equal to what found in the same setup for ergodic systems, *e.g.* dilute colloidal dispersion

References

[1] Priya R Banerjee, Anthony N Milin, Mahdi Muhammad Moosa, Paulo L Onuchic, and Ashok A Deniz. Reentrant phase transition drives dynamic substructure formation in ribonucleoprotein droplets. *Angewandte Chemie*, 129(38):11512–11517, 2017.

[2] Hendrik Christoffel Van de Hulst. *Light scattering by small particles*. Dover Publications, 1981.

[3] Mario Barbatti, Adelia JA Aquino, and Hans Lischka. The uv absorption of nucleobases: semi-classical ab initio spectra simulations. *Physical Chemistry Chemical Physics*, 12(19):4959–4967, 2010.

[4] Bruce J Berne and Robert Pecora. *Dynamic light scattering: with applications to chemistry, biology, and physics*. Courier Corporation, 2000.

[5] P-A Lemieux and DJ Durian. Investigating non-gaussian scattering processes by using nth-order intensity correlation functions. *JOSA A*, 16(7):1651–1664, 1999.

[6] Yeonee Seol, Gary M Skinner, and Koen Visscher. Elastic properties of a single-stranded charged homopolymeric ribonucleotide. *Physical review letters*, 93(11):118102, 2004.

[7] Yeonee Seol, Gary M Skinner, Koen Visscher, Arnaud Buhot, and Avraham Halperin. Stretching of homopolymeric rna reveals single-stranded helices and base-stacking. *Physical review letters*, 98(15):158103, 2007.

[8] David R Jacobson, Dustin B McIntosh, and Omar A Saleh. The snakelike chain character of unstructured rna. *Biophysical journal*, 105(11):2569–2576, 2013.

[9] Francesco Vanzi, Yasuharu Takagi, Henry Shuman, Barry S Cooperman, and Yale E Goldman. Mechanical studies of single ribosome/mrna complexes. *Biophysical Journal*, 89(3):1909–1919, 2005.

[10] Masao Doi and Samuel Frederick Edwards. *The theory of polymer dynamics*, volume 73. oxford university press, 1988.

[11] John G Kirkwood and Jacob Riseman. The intrinsic viscosities and diffusion constants of flexible macromolecules in solution. *The Journal of Chemical Physics*, 16(6):565–573, 1948.

[12] A Ziya Akcasu and Charles C Han. Molecular weight and temperature dependence of polymer dimensions in solution. *Macromolecules*, 12(2):276–280, 1979.

[13] Chi Wu and Shuiqing Zhou. Thermodynamically stable globule state of a single poly (n-isopropylacrylamide) chain in water. *Macromolecules*, 28(15):5388–5390, 1995.

[14] Stephen W Provencher. A constrained regularization method for inverting data represented by linear algebraic or integral equations. *Computer Physics Communications*, 27(3):213–227, 1982.

[15] A Scotti, W Liu, JS Hyatt, ES Herman, HS Choi, JW Kim, LA Lyon, U Gasser, and A Fernandez-Nieves. The contin algorithm and its application to determine the size distribution of microgel suspensions. *The Journal of chemical physics*, 142(23), 2015.

[16] SR Aragon and R Pecora. Theory of dynamic light scattering from polydisperse systems. *The Journal of Chemical Physics*, 64(6):2395–2404, 1976.

[17] David P Mascotti and Timothy M Lohman. Thermodynamic extent of counterion release upon binding oligolysines to single-stranded nucleic acids. *Proceedings of the National Academy of Sciences*, 87(8):3142–3146, 1990.

[18] M Thomas Record Jr, Timothy M Lohman, and Pieter De Haseth. Ion effects on ligand-nucleic acid interactions. *Journal of molecular biology*, 107(2):145–158, 1976.

[19] Shensheng Chen and Zhen-Gang Wang. Driving force and pathway in polyelectrolyte complex coacervation. *Proceedings of the National Academy of Sciences*, 119(36):e2209975119, 2022.

[20] Kathryn G Wilcox, Marlee E Dingle, Ankit Saha, Michael JA Hore, and Svetlana Morozova. Persistence length of α-helical poly-l-lysine. *Soft Matter*, 18(35):6550–6560, 2022.

[21] Hagen Hofmann, Andrea Soranno, Alessandro Borgia, Klaus Gast, Daniel Nettels, and Benjamin Schuler. Polymer scaling laws of unfolded and intrinsically disordered proteins quantified with single-molecule spectroscopy. *Proceedings of the National Academy of Sciences*, 109(40):16155–16160, 2012.

[22] Ofer Kimchi, Tristan Cragnolini, Michael P Brenner, and Lucy J Colwell. A polymer physics framework for the entropy of arbitrary pseudoknots. *Biophysical journal*, 117(3):520–532, 2019.

[23] Pierre-Gilles De Gennes. *Scaling concepts in polymer physics, Chapter X.2.4 for lattice polymers*. Cornell university press, 1979.

[24] Andrei Tokmakoff. *Concepts in biophysical chemistry, Chapter 7.3*. University of Chicago, 2021.

[25] Mark E Fornace, Nicholas J Porubsky, and Niles A Pierce. A unified dynamic programming framework for the analysis of interacting nucleic acid strands: enhanced models, scalability, and speed. *ACS Synthetic Biology*, 9(10):2665–2678, 2020.